SPATIAL RESOLUTION EFFECTS ON PIV MEASUREMENTS IN A TURBULENT WAKE FLOW

Keith Paschal[*] and Chungsheng Yao[*]
NASA LaRC, Hampton, VA
and
Scott Ullrich[†]
Illinois Institute of Technology, Chicago, IL

Abstract

The effects of spatial resolution on Particle Image Velocimetry (PIV) measurements obtained in the turbulent wake of a single-element airfoil were examined. Re_θ was approximately 2,000 for this particular wake flow. The objectives of the study were to improve PIV capability at high spatial resolution, and study high resolution turbulence velocity and vorticity measurements. Second-order turbulence moments were computed from 80 realizations at spatial resolutions of 0.942 and 0.566 mm, and compared with LDV measurements. Turbulent kinetic energy and velocity spectra were also computed for both spatial resolutions. Velocity structures, vorticity, and vorticity correlations from PIV measurements were examined from five realizations at spatial resolutions of 0.942, 0.566, and 0.419 mm. The second resolution of 0.566 mm corresponded to the Taylor microscale (λ) of approximately 0.66 mm and the highest resolution was constrained by the interrogation volume requirement of at least 10 particle pairs. Results indicate that second order moments were resolved at the lowest resolution and that large eddies were well resolved when the spatial resolution was approximately λ. Although vorticity magnitudes at 0.419 mm were on the order of theoretical values, improved resolution would be required to fully resolve the vorticity field for this flow. The cost in time for each spatial resolution was also contrasted with respect to gain.

Nomenclature

c	airfoil chord
d_τ	particle image diameter on CID array
d_{pix}	CID pixel diameter
k_x	wavenumber in x-direction
l_{mv}	length of square interrogation area
ℓ	integral length scale
Re	Reynolds number
R_{uu}, R_{vv}	spatial velocity autocorrelations
$R_{\omega\omega}$	spatial vorticity autocorrelation
S_{uu}, S_{vv}	spatial velocity spectra
u, v	instantaneous velocity components
U, V	mean velocity components
u', v'	fluctuating velocity components
u'_{rms}, v'_{rms}	rms turbulence intensities
<u'v'>	Reynolds stress
x, y	streamwise and wall-normal coordinates
Δ	displacement of double-exposed particle images
η	Kolmogorov microscale
θ	momentum thickness
λ	Taylor microscale
$\omega_\mathbf{z}$	spanwise vorticity
∞	denotes freestream condition
< >	ensemble average

---

[*] Aerospace Engineer, Member AIAA, Experimental Flow Physics Branch

[†] Research Assistant, Member AIAA, Illinois Institute of Technology

Introduction

Over the past two years the Experimental Flow Physics Branch at NASA Langely Research Center has developed a photographic-based PIV system to support fluid mechanics research. This system was recently employed to investigate the 2–D turbulent wake of a single-element airfoil (Yao and Paschal[1]). The 2–D airfoil wake provided a practical validation test for the PIV system in which 240 realizations were processed and analyzed. The present work focused on the same data set, but set out to determine what effect spatial resolution had on PIV turbulence and vorticity measurements and, in the process, improve PIV capability at high resolution.

This study consisted of two parts. First, turbulence statistics and spectra were compared at 0.942 and 0.566 mm resolutions in the x and y- directions. 80 pictures were interrogated at a spatial resolution of 0.566 mm (~ λ) in order to assess the effect of resolution on statistical information. The computed second order moments were then compared with statistical data from the original interrogations performed at a nominal spatial resolution of 0.942 mm (Yao and Paschal[1]). These statistics were also compared with LDV data obtained on the same airfoil configuration. In addition, 2–D turbulent kinetic energy and 1–D velocity spectra were examined. Second, velocity and vorticity structures, and length scales were examined at spatial resolutions of 0.942, 0.566, and 0.419 mm in the x and y-directions. Five pictures were interrogated at 0.419 mm spatial resolution in order to make the comparisons. The highest resolution was constrained by seeding density requirements from the conclusions of Keane and Adrian[2].

It is important to recognize that resolution in the spanwise direction was fixed for this study. PIV employs a light sheet with a fixed thickness to illuminate particles tracking the flow. An imaging lens is used to record the particle images. This lens integrates over the thickness of the light sheet to produce a 2–D picture of the double-exposed particles. In this study particular PIV pictures were interrogated at three spatial resolutions in the x and y-directions with a resolution of about 0.5–0.7 mm in the spanwise direction.

Vorticity was of great interest as the production of turbulence is related to vorticity stretching by the fluctuating rate of strain. The Taylor microscale is the length scale associated with vorticity as λ is proportional to the gradients in the flow. Adrian[3] states that spatial resolution should be many times smaller than λ to resolve the velocity gradients in the flow. Although the limiting resolution of 0.419 mm was not small enough to accurately resolve λ, important trends concerning vorticity magnitude and integral scales were extracted.

Experimental Description

Experimental Setup

PIV measurements were made in a 108x254 mm closed-return low-speed wind tunnel in the turbulent wake of a single-element airfoil (figure 1.) A natural laminar flow airfoil, with a 101.6 mm chord and 12.7 mm thickness, was mounted approximately 50.8 mm above the tunnel floor at 4.5° angle of attack. The freestream velocity of 18.1 m/sec yielded a Re_c of 135,000 and Re_θ of 2,000. A TSI six jet atomizer was used to generate high concentrations of seed particles. The resulting mineral oil particles had an average diameter of about 0.3 μm according to TSI specifications. The largest particles were able to track turbulent eddies within 5% of the velocity difference across the wake.
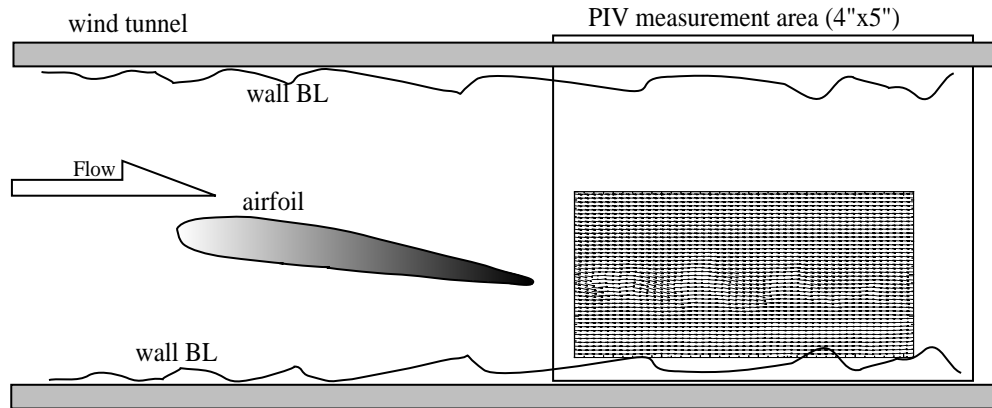

Figure 1. Experimental configuration.

The intent of the study was to investigate the effects of spatial resolution on PIV measurements and not to provide quantitative data on airfoil wake flows. As a result, tunnel flow uniformity and quality were not priorities. The effective angle of attack of the model was lower than 4.5º due to streamline confinement, and blockage from the model, model mount, and tunnel boundary layers resulted in a 20% increase in U relative to upstream conditions. The high frequency, turbulent structures were thought to be unaffected by low frequency oscillations (< 1 Hz) observed in the LDV data. Freestream turbulence levels were on the order of 1.5%.

PIV System

In this section our PIV system will be briefly described. A more detailed explanation of the optical setup and operation is given in Yao and Paschal[1]. Reviews by Adrian[3] and Buchave[4] provide general information on PIV and its status. This section will cover our lasers and optics, camera and image shifting technique, and interrogation hardware. Interrogation software will be covered in the next section.

Two Nd:Yag lasers illuminated the test plane with approximately 500 mJ energy output per pulse at 532 nm wavelength. The optical table layout of the Yag lasers and optics is shown in figure 2. The second Yag was oriented 22.5º from the first so that its beam could be combined at the polarizer while maintaining right angle mirror reflections. A half-wave plate was used to rotate the polarization of the second beam 90º relative to the first beam. Cross-polarization between the two beams was required for the image shifting technique which removed flow direction ambiguity. After beam combination at the polarizer a light sheet with adjustable focal length, width, and thickness was formed. For this test the light sheet in the test section was 150 mm wide and less than 1 mm thick according to burn marks. The waist thickness according to Gaussian beam propagation was 0.371 mm. The laser pulse separation was 11.0165 ± 0.001 μs and the duration of each pulse was between 5 and 7 ns.

M: mirror
P: polarizor
A: aperture
G: glass
GL: ground glass
SL: spherical lens
LL: spherical lens
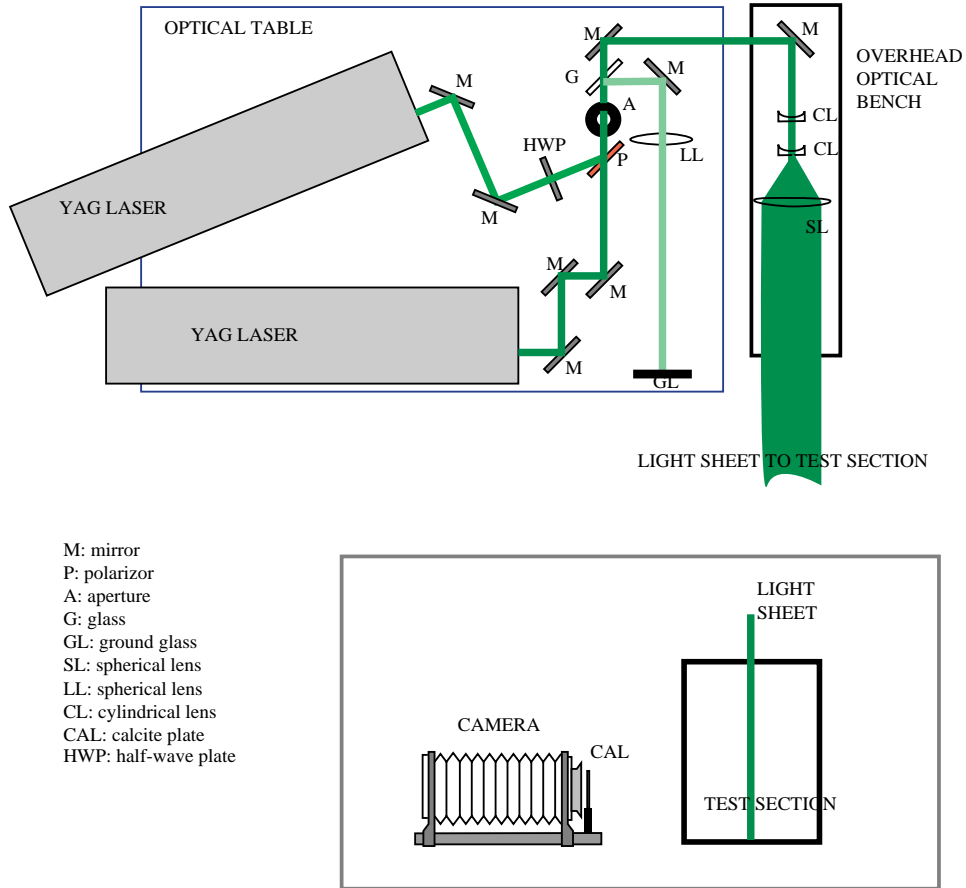CL: cylindrical lens
CAL: calcite plate
HWP: half-wave plate

Figure 2. Laser and optics setup.

A 4"x5" format camera with a 300 mm focal length processor lens was used to record particle images at 1:1 magnification. The long focal length lens was used to minimize the out-of-plane displacement error and the measurement area covered up to 120x100 mm at 1:1 imaging. A 25 mm square calcite crystal was placed in front of the camera to remove flow direction ambiguity. The 1.3 mm thick calcite plate removed flow direction ambiguity by shifting the vertically polarized beam downward 0.13 mm. The specifications of the plate followed the design of Landreth and Adrian[5]. The exposure of micron-sized oil particles at an aperture setting of f/16 was satisfactory at maximum laser energy output. The particle images were recorded on TMAX 400 film and measured 20–30 μm in diameter. These images were almost aberration-free and showed negligible geometry distortion.

Double exposed particle images were analyzed on a UNIX workstation. A CID (charge injection device) camera with a resolution of 512x512 pixels and 50 mm enlarger lens sampled images from a small portion (approximately 3.5 mm square) of the PIV photograph. The interrogation camera was calibrated using a grating pattern of 100 lines per inch and the accuracy of the interrogation magnification was within 0.5%. A frame grabber transferred the particle images to the interrogation computer which incorporated an i860 high-speed floating-point processor to compute image cross-correlations of a sub-region of the sampled frame. The size of the sub-region defined the PIV interrogation area and spatial resolution. Square interrogation areas of 0.942mm x 0.942mm, 0.566mm x 0.566mm, and 0.419mm x 0.419mm were evaluated in this study.

PIV Interrogation Software

PIV data at 0.942 mm resolution were interrogated with a cross correlation technique that shifted the second image with respect to the first image by 18 pixels in the y-direction. This shift corresponded to that imposed by the calcite crystal. Since there was no shift in the x-direction, the displacement of the double exposed images relative to the length of the interrogation area (Δ/l_{mv}) was held < 0.25 as suggested by Keane and Adrian[2] to reduce velocity bias in regions of large velocity gradients. The cross-correlation was computed on a 128x128 pixel area and took approximately 0.080 seconds. Nyquist sampling criterion required over-sampling of the interrogation area by 50%. More detailed information was given in Yao and Paschal[1]. Figure 3(a,b) shows an example of an instantaneous velocity field and its corresponding fluctuating field. 240 realizations were used to compute the ensemble mean from which the fluctuating field

was extracted. The origin in figure 3 was located at the airfoil trailing edge.

The correlation technique used at the higher resolutions cross-correlated the first particle image with the second image which was shifted in both the x and y-directions. Shifting in the x-direction was required as $\Delta/l_{mv} > 0.25$. The vertical offset corresponded to the calcite shift and the horizontal offset corresponded to the mean velocity across the wake. Since a variable shift correlation technique (see Meinhart, et al[6]) had not yet been incorporated, the window offsets in both directions were fixed. Once again, the cross-correlations were computed on a 128x128 pixel area and 50% oversampling of the interrogation area was performed. Therefore, computation time per vector was the same for all three resolutions.

Prassad, et al[7] suggest that the ratio of the number of pixels per particle image (d_τ/d_{pix}) be approximately 4 to optimally reduce bias and random errors in the computation of the correlation peak location. Bias errors arise when particle images are poorly resolved by the video camera pixel array. Random errors are proportional to d_τ. Therefore, d_τ/d_{pix} of approximately 4 is a compromise between the limiting extremes of both errors. These findings apply when a centroidal technique is used for detection of the correlation peak. We have used these findings as rough guidelines, despite the fact that our code used a parabolic curvefitting technique, since the work by Prassad is the only available reference known to the authors.

A comparison of selected interrogation parameters is presented in Table 1. As d_τ/d_{pix} increased with resolution the random error in the measurements also increased. A factor of 4 increase in speed could have been achieved by fixing d_τ/d_{pix} at approximately 4 and performing 64x64 pixel cross-correlations at the higher resolutions. More will be said on this subject later in the paper. Vector validation rate and signal to noise ratio varied with the number of particles in each interrogation spot. It is important to note that the percentage of erroneous vectors ($\leq 1\%$) did not change as the number of particles decreased from 47 to 22. The highest spatial resolution was constrained by seeding density. At a resolution of 0.419 mm the number of image pairs had dropped to approximately 12 (Keane and Adrian[2] suggest ≥ 10–15). The total number of vectors for each resolution is also shown for comparison.

A semi-automated post-interrogation code was used to remove erroneous vectors. A 3x3 binomial filter was used to smooth the instantaneous velocity fields and remove random high-frequency noise. Mean and turbulence statistics, vorticity, various spectra and correlations were then computed.

(a) Instantaneous Flow Field

(b) Fluctuating Flow Field
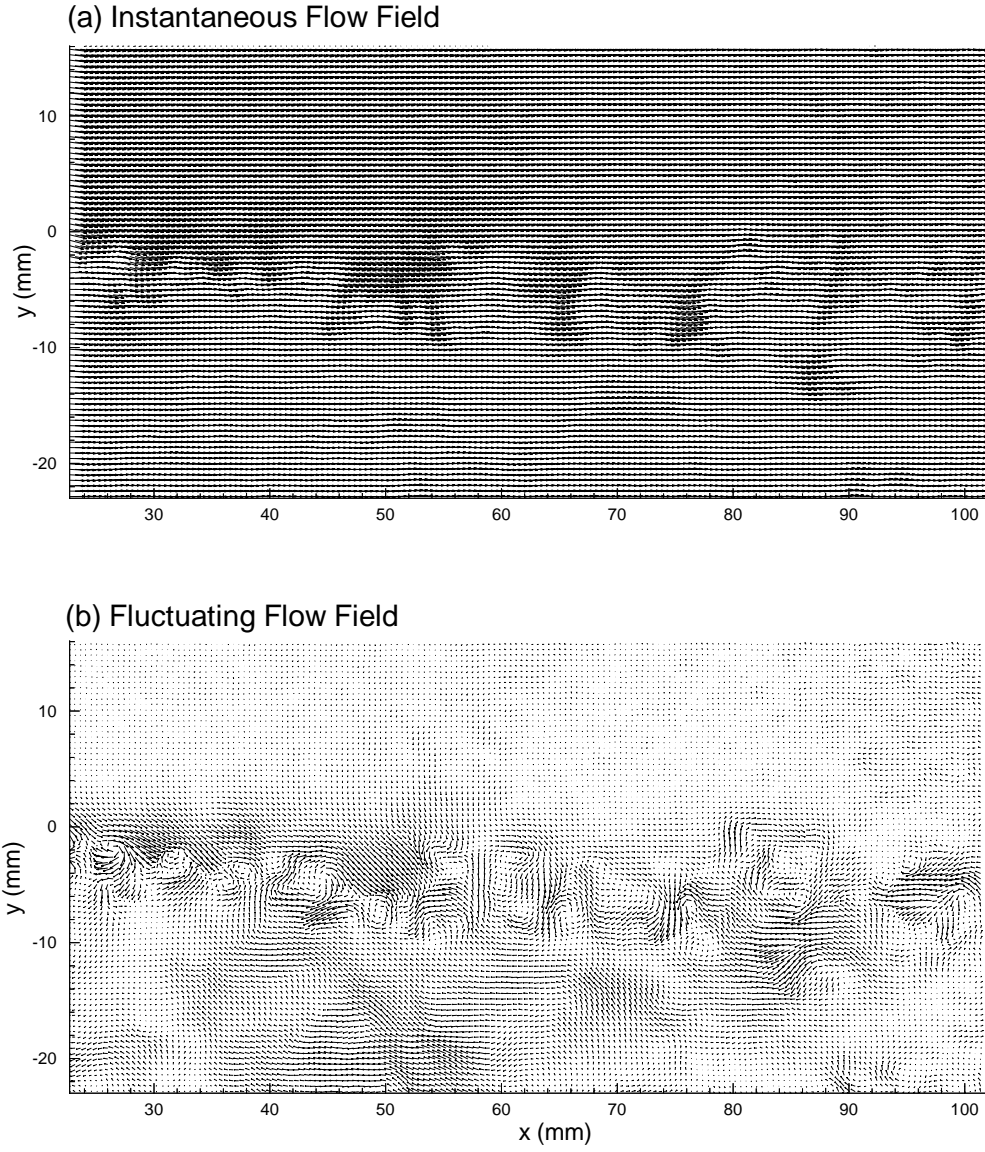
Figure 3. Instantaneous and fluctuating vector maps (spatial resolution = 0.942 mm).

spatial resolution (mm)	$\frac{d_\tau}{d_{pix}}$	Vector validation rate	# of particles in interrogation spot	signal/noise	# of grid points
0.942	4.1	99+%	47±13%	4.70	15,792
0.566	6.8	99+%	22±13%	1.54	28,728
0.419	9.2	96+%	12±13%	1.35	50,400

Table 1. Interrogation parameters.

Results and Analysis

Turbulence Statistics and Spectra

Mean profiles obtained at three downstream locations are presented in figure 4. PIV results were acquired from 80 realizations at resolutions of both 0.942 and 0.566 mm. LDV data was acquired with a 2–component system from 4K data points. LDV measurement volume was approximately 2.5 mm in the spanwise direction and 0.13 mm in both the x and y-directions. Fairly good agreement was seen to exist between PIV and LDV measurements. Note that data from both systems was obtained on the same configuration, but it was not feasible to acquire the data simultaneously.

A comparison between PIV and LDV turbulence second order moments is shown in figure 5. The apparent noise increase at 0.566 mm may be due to an inadequate number of realizations; note that the two resolutions converge in the freestream. LDV measurements indicated a slightly wider wake than those from the PIV system. Despite poor tunnel flow, first order agreement existed between PIV and LDV second order moments. The turbulent kinetic energy was computed in the 2–D sense as the spanwise velocity component could not be measured with conventional PIV. The energy increase at 0.566 mm indicated that the ability to measure energy in the smaller scales of motion existed with increased resolution.

1–D velocity spectra computed along the centerline of the wake from 80 realizations is shown in figure 6. The energy increase seen in both $\langle S_{uu} \rangle$ and $\langle S_{vv} \rangle$ was related to the turbulent kinetic energy increase in figure 5(d). Once again the ability of the instrument to measure the energy in the smaller scales has been shown. The energy difference was due to the contributions of turbulent eddies $\leq$ 3–4 mm in diameter near the wake centerline which were resolved more accurately at 0.566 mm resolution. The oscillating behavior of v' is clearly shown by the peak in $\langle S_{vv} \rangle$ at k_x of approximately 0.06. These wavy v' patterns had an approximate wavelength of 17 mm.
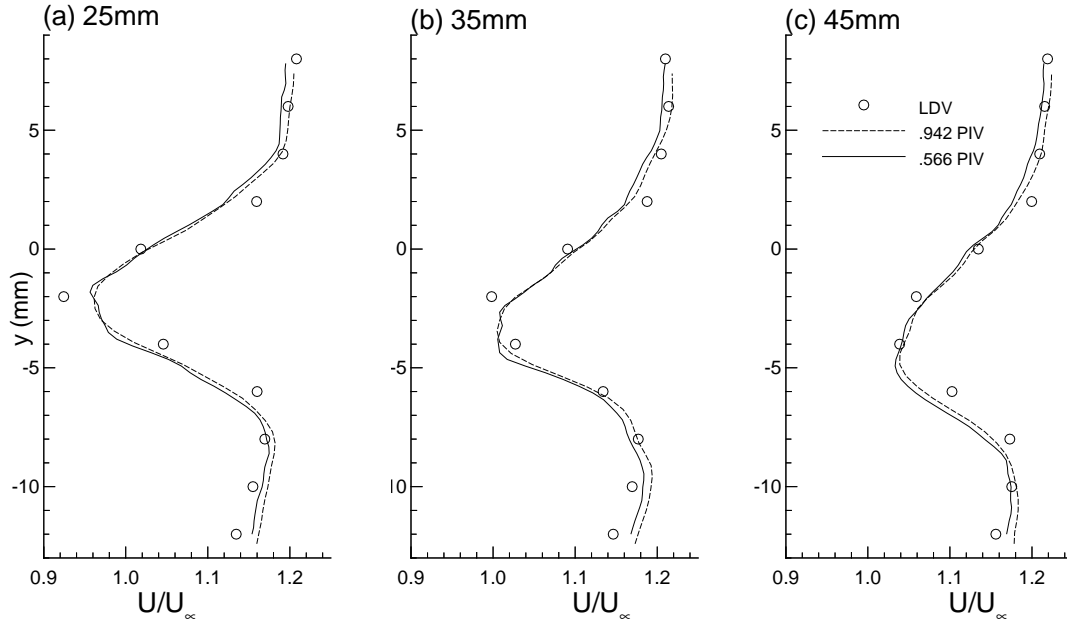

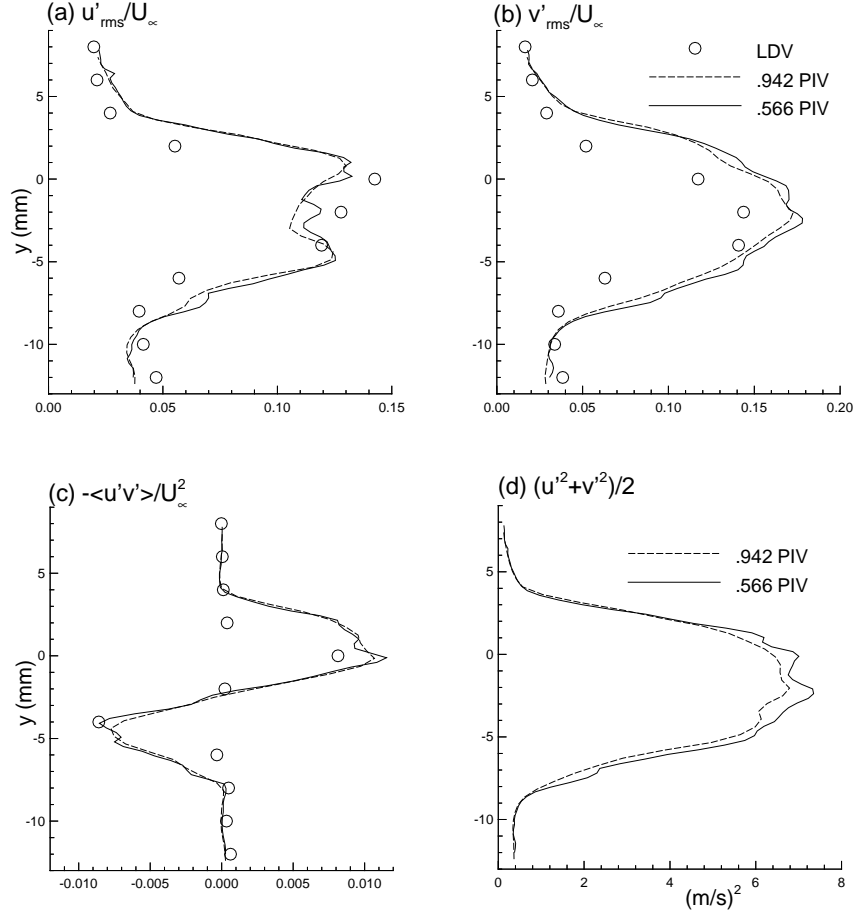**Figure 4. PIV and LDV mean profile comparison (80 realizations).**

6

Figure 5. PIV and LDV second order turbulence statistics and energy comparison (80 realizations).
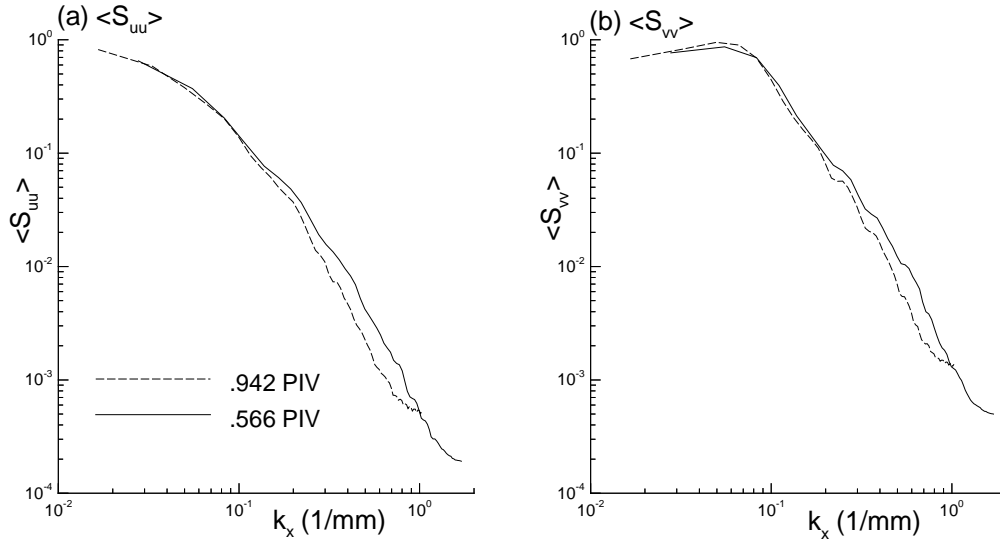

Figure 6. Effect of spatial resolution on 1–D velocity spectra computed along the wake centerline (80 realizations).

Turbulent Scales of Motion

Relevant length scales for the turbulent wake flow were estimated based on integral scales computed from the 2–D correlations in figure 7. The correlations were computed from 240 realizations over a wake area of 80 mm x 45 mm. All the relevant scales were less than 20 mm and the correlations in figure 7 are presented in this scale range. Since our goal was to obtain average integral scales over the entire field, FFTs were used in the interest of time despite the inhomogeneous flow field. The oscillating behavior of v' was again seen in the 2–D $<R_{vv}>$ contour.

Table 2. presents a summary of the various length scales associated with both integral scales detected in the wake. ℓ_u and ℓ_v were computed by integrating $<R_{uu}>$ and $<R_{vv}>$ in both the x and y-directions. For example, ℓ_{ux} was computed by integrating $<R_{uu}(x,0)>$ in the streamwise direction. ℓ_{ux} and ℓ_{vy} were approximately equivalent and ℓ_{uy} and ℓ_{vx} were also equivalent leaving two integral scales of motion. The smaller integral scale of 2.8 mm was taken from the value of ℓ_{uy} and the larger from ℓ_{vy}. The Taylor and Kolmogorov scales were estimated using the standard high Reynolds number relations based on Re_ℓ[8]:

$$\frac{\lambda}{\ell} \sim \left(\frac{15}{Re_\ell}\right)^{\frac{1}{2}}$$

$$\frac{\lambda}{\eta} \sim (225 Re_\ell)^{\frac{1}{4}}$$

The gradient scales were 4–6 times smaller than the corresponding integral scales and the dissipation scales were an order of magnitude less than the corresponding Taylor microscales.

Of particular interest in this study from a conservative point of view was the ability, or lack thereof, to resolve the gradient scale estimated from the smallest computed integral scale. The Kolmogorov scale for this particular configuration was beyond the reach of even high magnification PIV. Resolution of the integral scale implied resolution of the large eddies in the flow, and the ability to accurately compute velocity gradients (hence vorticity) would be implied by resolution of λ. Note that all three spatial resolutions compared were on the order of λ.

ℓ (mm)	Re_ℓ	λ (mm)	η (mm)
2.8	270	~0.66	~0.04
5.4	520	~0.92	~0.05

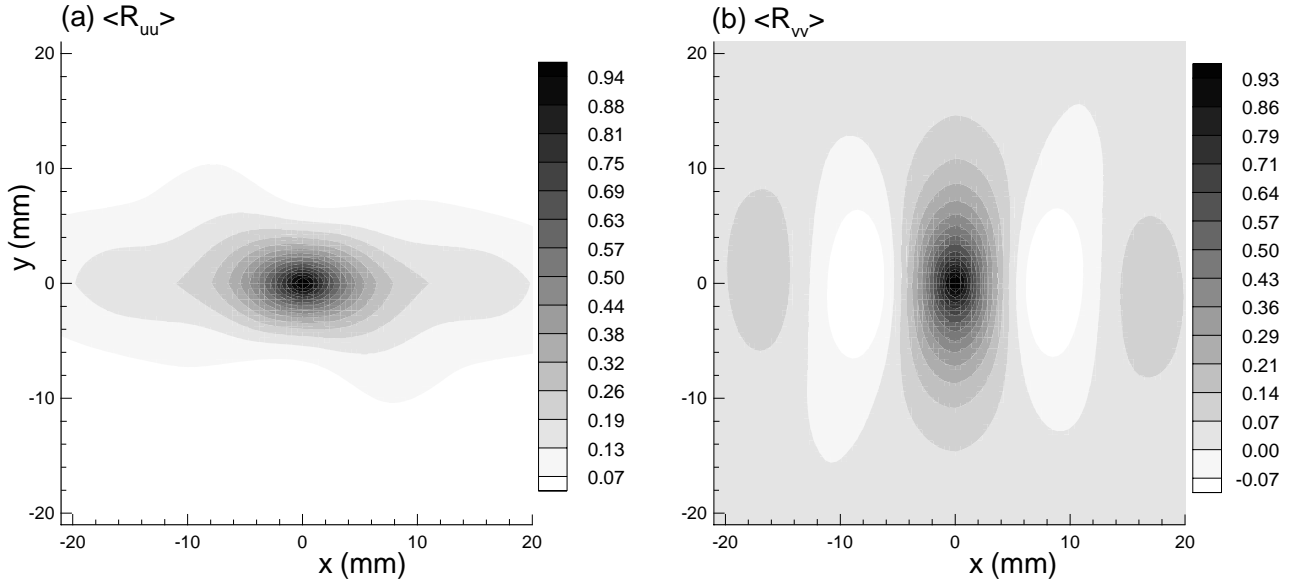**Table 2. Relevant turbulent scales.**

Figure 7. 2–D velocity correlations (240 realizations).

8

Velocity and Vorticity Structures

The effect of spatial resolution on the wake fluctuating velocity field is shown in figure 8. The fluctuating field was computed by subtracting out a reference velocity such that the vector field was observed in a moving frame. This global average velocity was used as opposed to the ensemble average because only 5 pictures were interrogated for the highest resolution due to time constraints. More PIV realizations would be required to provide a good statistical average for the computation of the mean flow. The increase in vector density is clearly shown between the 0.942 and 0.419 mm cases.

Instantaneous vorticity maps corresponding to the three cases in figure 8 are shown in figure 9. Out of plane vorticity (ω_z) was determined by employing Stoke's theorem to compute the circulation about each grid point as described in Landreth and Adrian[9] and Reuss, et al[10]. This integration method provided built in smoothing over the interrogation area. Two trends from the ω_z contours were expected and important. First, the size of the vorticity regions decreased with spatial resolution, and second, the magnitude of ω_z increased with spatial resolution.

The effect of spatial resolution on velocity structure is clearly shown in figure 10. Two examples of differences in the wake features can be seen between the higher resolutions and the nominal resolution of 0.942 mm. In the upper right hand region (x ~ 43 and y ~ –3) three individual vortical structures appeared at the higher resolutions of 0.566 and 0.419 mm. At the nominal resolution these structures were averaged into a single vortical structure. Slicing through the middle of the wake (x ~ 41 mm) a region of fairly strong upflow existed. This upflow pattern turned slightly right of vertical before curling into the upstream direction. The 0.942 mm resolution was unable to resolve the overshoot and predicted a vertical flow pattern. A resolution of approximately λ (in this case ~ $\ell/4$) was sufficient to resolve the large eddies embedded in the flow.

The effect of resolution on an average wake vorticity was also examined. The value of vorticity squared was computed by averaging over the 2–D wake area from a single realization. Four different techniques were used to compute this average vorticity as shown in figure 11. The techniques were 2nd and 4th order finite difference, 4th order convolved with a 3x3 binomial filter, and the circulation method discussed earlier. Vorticity squared increased with spatial resolution as was shown from the vorticity contours. Estimates of $\overline{\omega_z \omega_z}$ from the isotropic relationship given in Batchelor[11] were approximately 2.2 x 10^7 where:

$$\overline{\omega_i \omega_i} = 15 \frac{\mathbf{u}^2}{\lambda^2}$$

$$\mathbf{u}^2 = \frac{1}{3} \overline{u_i u_i}$$

Although 0.419 mm resolution was not enough to completely resolve out of plane vorticity, our measurements were on the correct order of magnitude. Also note that the finite difference techniques yielded larger values than the integral technique which incorporated some smoothing.

As resolution of the gradients was improved one would expect the average vorticity magnitude to gradually roll-off and approach the true value. The opposite effect (figure 11) was due to amplification of increased random noise present at higher resolutions during the computation of vorticity. As previously mentioned, the optimum reduction of both bias and random errors occurred when d_τ/d_{pix} was approximately 4 (see Prassad, et al[7]). As this ratio increased for the higher resolutions the random error dominated while the bias error became negligible. The Solid circles in figure 12 are the freestream measurements of vorticity and provide an estimate of associated noise. The corrected average wake vorticity (denoted by hollow squares) was determined by subtracting out the estimated freestream vorticity. More data points would be needed in order to determine the resolution trend more accurately. The circulation technique was used to compute the average vorticity of figure 12.

A vorticity integral scale (ℓ_ω) was used to quantify the scales associated with vorticity structures seen in the vorticity contours (figure 9). 2–D vorticity autocorrelations were computed and averaged over the five realizations to determine the average vorticity scale across the wake. $R_{\omega\omega}(x,0)$ and $R_{\omega\omega}(0,y)$ are shown in figure 13. Vorticity was originally computed from the circulation method. The qualitative observations from the vorticity contours were confirmed by these quantitative results.

The effect of resolution and vorticity computational techniques on ℓ_ω is shown in figure 14. The limiting value for the measured integral scale is denoted by the solid line which is spatial resolution plotted against itself. ℓ_ω is shown to scale with spatial resolution. This trend reinforced the earlier conclusion that λ was not fully resolved at 0.419 mm. Once again, more data points would be needed to further quantify the ℓ_ω trend.

The three components of the 2–D Reynolds stress tensor and turbulent kinetic energy are shown in figure 15 as a function of spatial resolution. The values were computed by averaging across the wake for a single realization. These statistics show little dependency upon spatial resolution as discussed earlier.
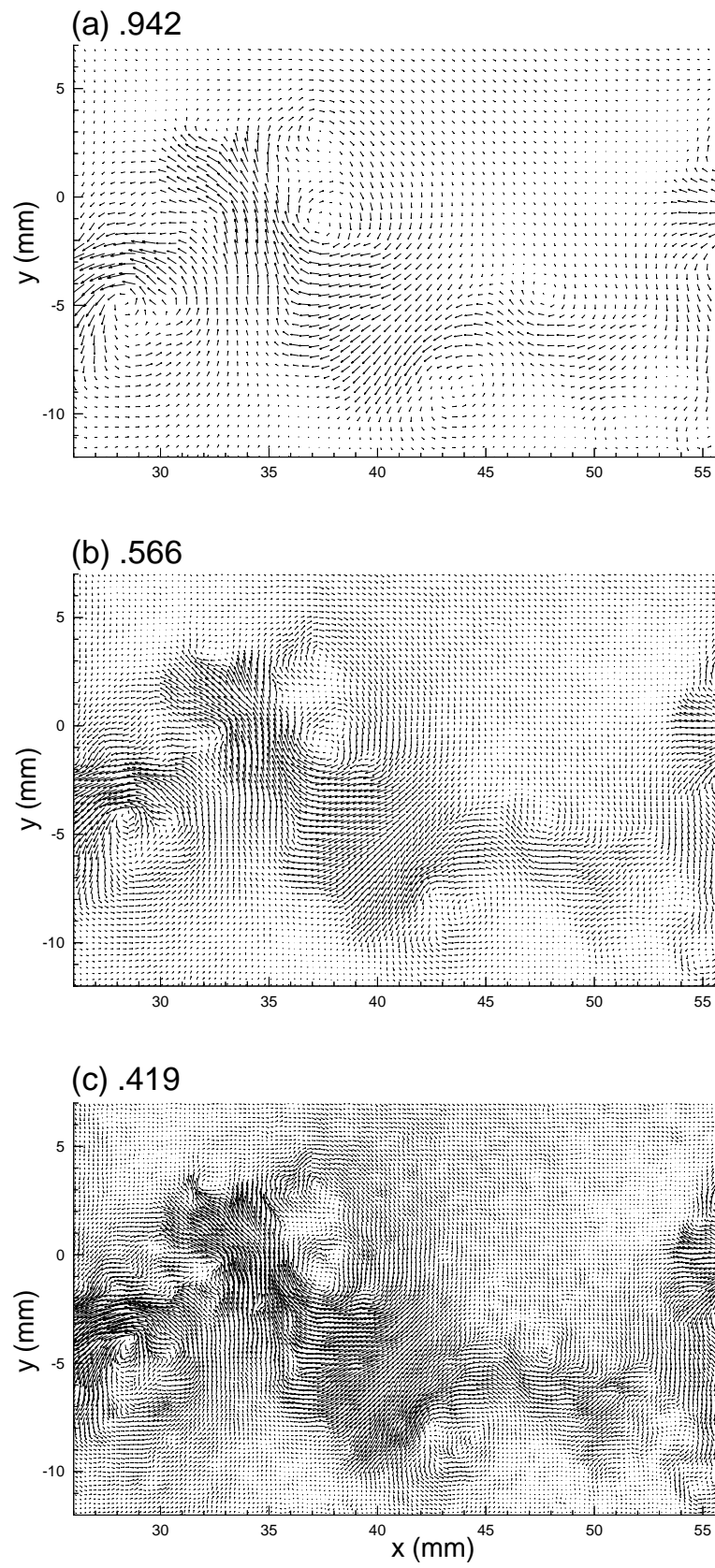
(a) .942

(b) .566

(c) .419

x (mm)

Figure 8. Effect of spatial resolution on fluctuating velocity field.

10
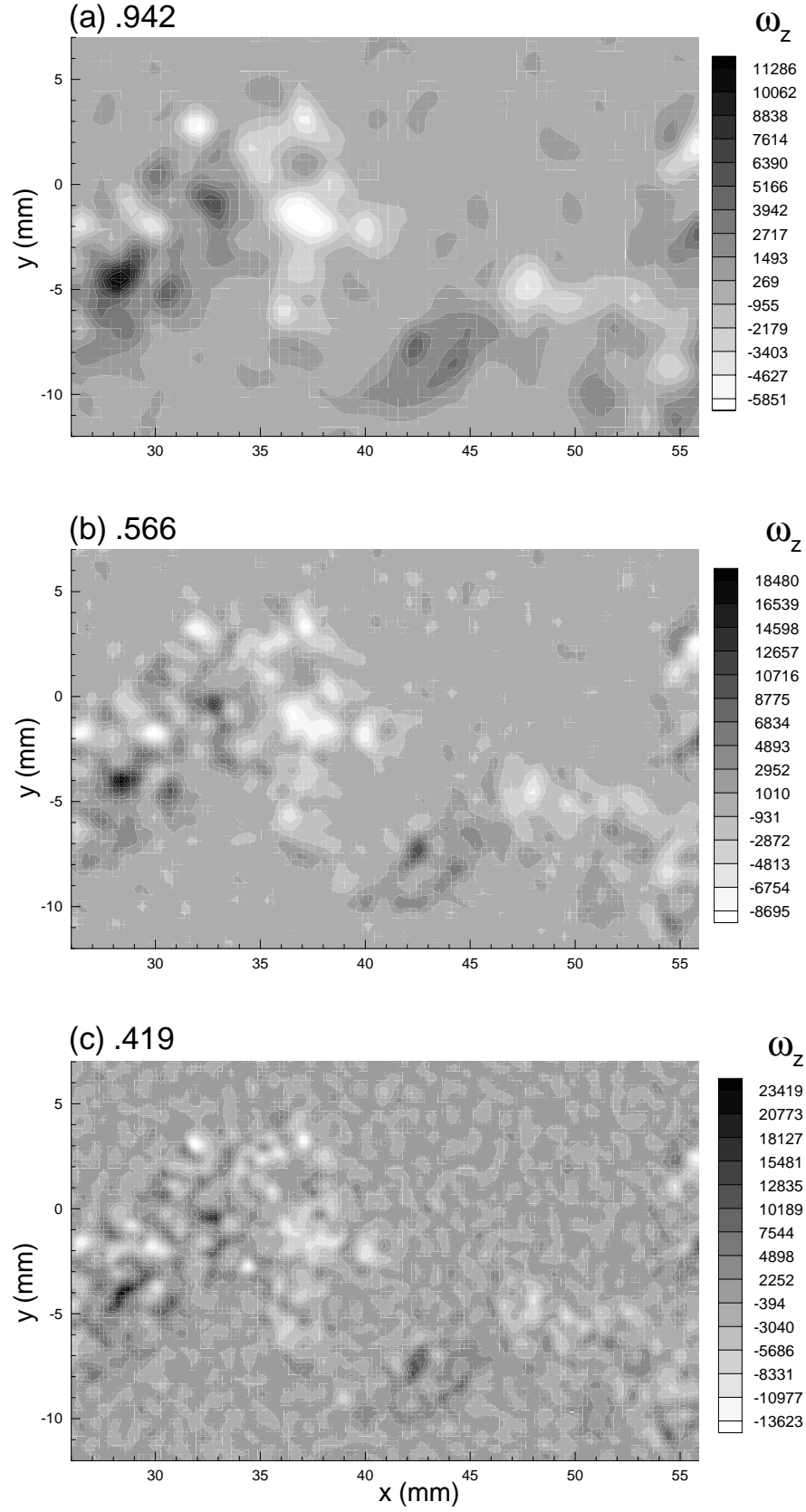
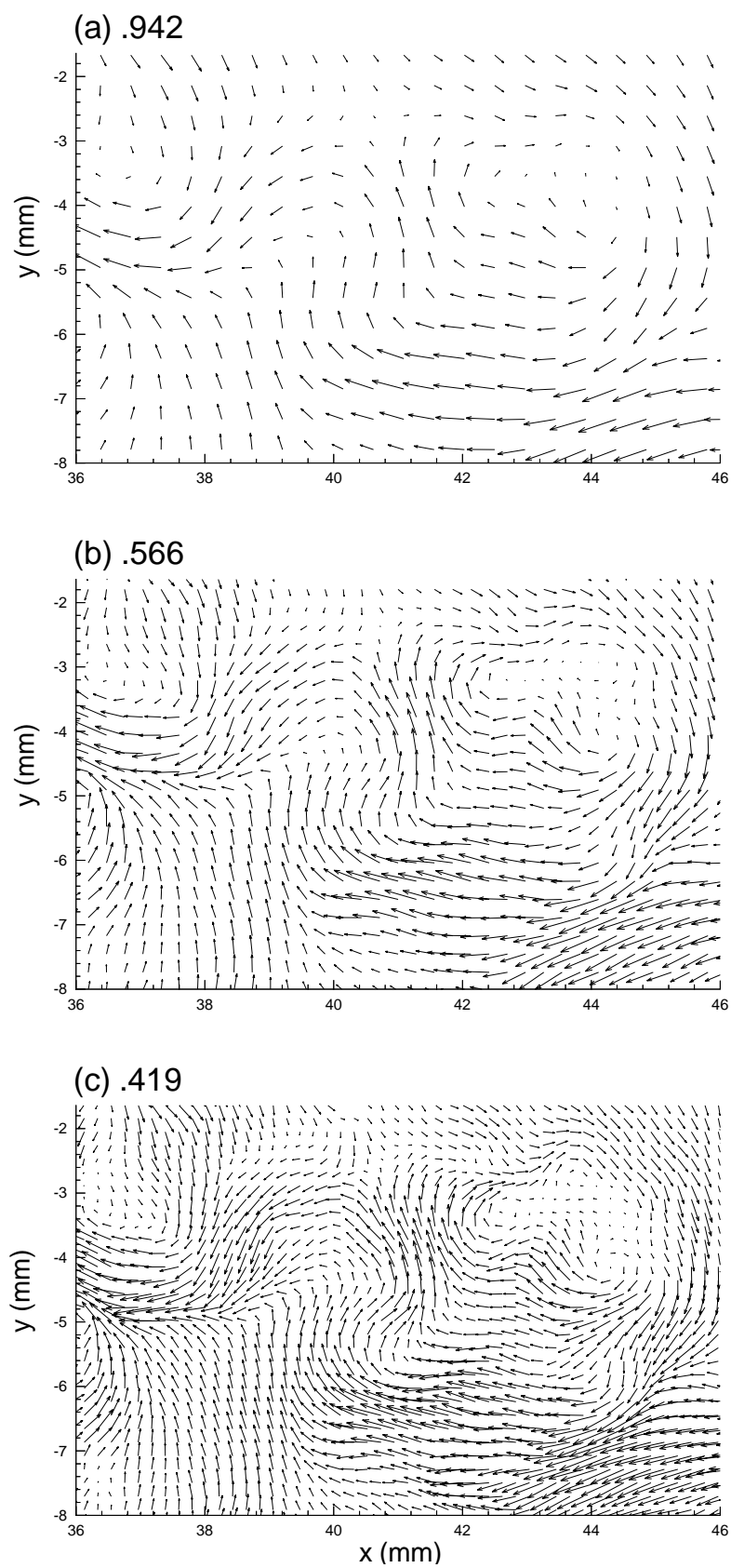**Figure 9. Effect of spatial resolution on instantaneous vorticity field.**

11

(a) .942

(b) .566

(c) .419

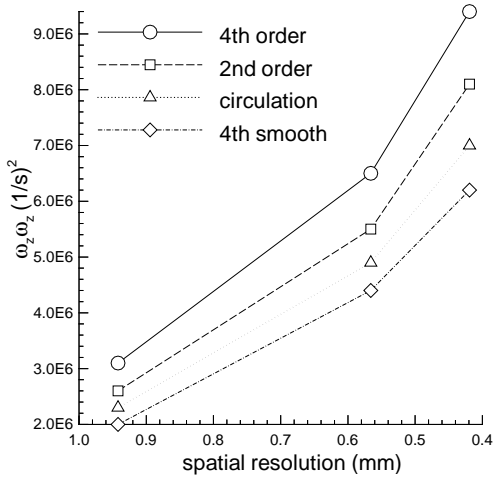**Figure 10. Effect of spatial resolution on fluctuating velocity field.**

Figure 11. Effect of spatial resolution on average vorticity.

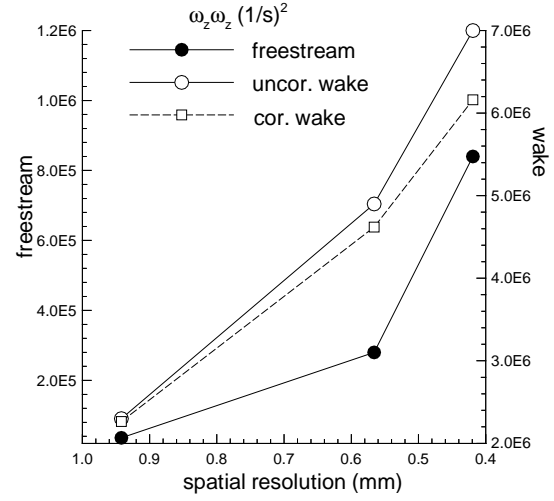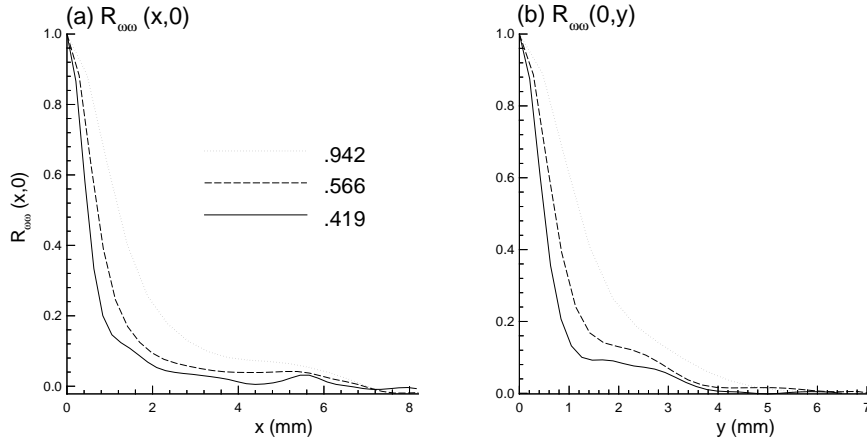**Figure 12. Effect of random noise on average vorticity.**

Figure 13. Effect of spatial resolution on vorticity autocorrelation.
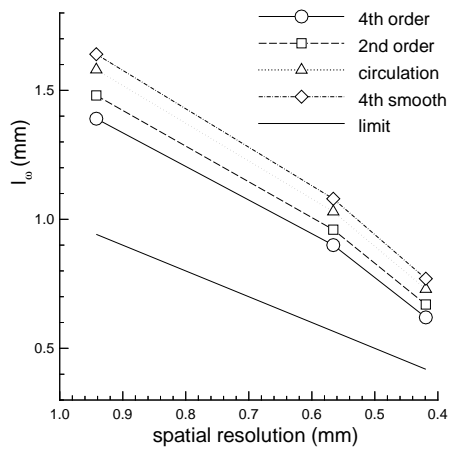

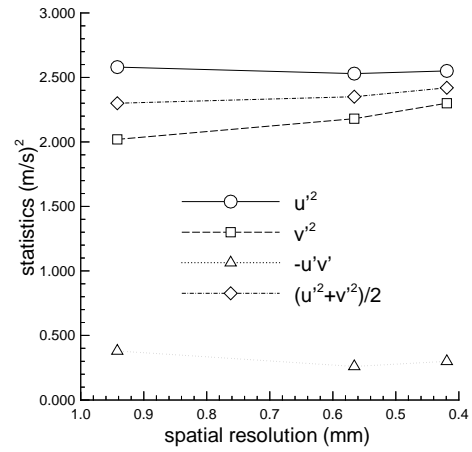**Figure 14. Effect of spatial resolution on vorticity integral scale.**

Figure 15. Effect of spatial resolution on second order turbulent statistics and energy.

Tradeoffs and Cost

The cost in time associated with each spatial resolution is tabulated in table 3. Computer time is a measure of the speed of the interrogation program and human time is associated with the interactive aspects of the vector validation process. Both were dependent on the total number of vectors processed while computer time was also dependent upon the size of the correlation arrays. Computer time, relative to human time, may not appear to be an important factor, but if one has 200+ pictures at high resolution the interrogation process may take weeks. The question is one of cost versus benefit.

spatial resolution, 128x128 pixel correlations (mm)	computer time (factor)	human time (factor)
0.942	1.0	1.0
0.566	2.5	2.5
0.419	4.5	4.5

Table 3. Cost of increased spatial resolution.

The optimum resolution depends upon the questions being asked about a particular flow and what tradeoffs one is willing to make. Accurate statistics do not require high resolutions relative to vorticity measurements and may be performed with a smaller time penalty. Better resolution of the integral scales is required for adequate resolution and identification of velocity structures. Contributions to Reynolds stress, turbulent kinetic energy, etc. from velocity structures could then be determined through conditional or phase averaging. Given a large field of view, the tradeoff is an increased cost in time. For our particular flow and interrogation parameters, attempted resolution of the gradient scale is pointless (take note that only 5 pictures were interrogated at 0.419 mm resolution). If vorticity measurements are required, high magnification PIV must be performed over a smaller field of view to combat the ever increasing time penalty.

Interrogation software with the ability to change the correlation pixel array size and employ a variable, or adaptive cross correlation technique[6] would be required for efficient measurements at high resolutions. For example, using 64x64 pixel correlation arrays would lower the required computer time by a factor of 4 and reduce random noise. The computer time required for 64x64 correlations at 0.419 mm resolution is now on the order of that required for 128x128

pixel correlations at 0.942 mm. Human time requirements remain the same (table 1.) since the total number of vectors for both resolutions also remains the same. The random noise should also be on the same order of the 128x128 pixel correlations at 0.942 mm as d_τ/d_{pix} would be approximately 4. Modifications to our software are currently underway.

Conclusions

Spatial resolution effects on PIV measurements in the wake of a single element airfoil at 4.5° angle of attack were investigated. The freestream velocity was 18.1 ms, Re_θ was approximately 2,000, and Re_c was 135,000. Vector validation rates from 96% up to 99% were achieved due to high image density of mineral oil particles with a 0.3 μm average diameter. Second order turbulent moments, turbulent kinetic energy, and velocity spectra were compared at resolutions of 0.942 and 0.566 mm. LDV measurements of the second order turbulent moments were compared with those from the PIV measurements. Velocity and vorticity structures were compared at spatial resolutions of 0.942, 0.566, and 0.419 mm. Significant conclusions from this study are listed below:

1. The lowest resolution (0.942 mm) was adequate for the measurement of the mean flow and second order turbulence moments. PIV measurements were in agreement with LDV measurements of the mean and second order statistics to the first order.

2. Spatial resolution of approximately λ (for our particular flow $\lambda \sim \ell/4$) was required to resolve the large eddies in the flow.

3. At the highest resolution (0.419 mm) vorticity magnitudes were on the order of theoretical estimates. However, full vorticity resolution was not achieved at this recording magnification as values of ℓ_ω and $\overline{\omega_z\omega_z}$ did not converge as resolution increased. Vorticity computations in the freestream showed increased random noise at higher resolutions due to increased values of d_τ/d_{pix}.

4. The optimum resolution for this study at 1:1 recording magnification and 128x128 pixel resolution was 0.566 mm ($\sim \lambda$). This was in fact the point of diminishing return as the highest resolution of 0.419 mm was unable to fully resolve vorticity and carried too great a computer cost.

5. For high resolution PIV, holding $d_\tau/d_{pix} \sim 4$ by reducing the size of the correlation arrays should yield faster interrogation turnaround times and optimally reduce both bias and random errors.

14

References

1. Yao, C.S., and Paschal K.B.; PIV Measurements of Airfoil Wake-Flow Turbulence Statistics and Turbulent Structures. AIAA 94–0085, 32nd Aerospace Sciences Meeting and Exhibit, Jan 10–13, 1994, Reno, NV.

2. Keane, R.D., and Adrian, R.J.: Optimization of Particle Image Velocimeters Part I: Double Pulsed Systems. Meas. Sci. Technol., 1, 1990, 1202–1215.

3. Adrian, R.J., Particle-Imaging Techniques for Experimental Fluid Mechanics. Annual. Review Fluid Mech., 23, 1991, 261–304.

4. Buchave, P.: Particle Image Velocimetry-Status and Trends. Exp. Thermal and Fluid Sci., 5, 1992, 586–604.

5. Landreth, C.C., and Adrian, R.J.: Electrooptical Image shifting for particle image Velocimetry. Applied Optics, 27, 1988, 4216–4220.

6. Meinhart, C.D., Prassad, A.K., and Adrian, R.J.: A Parallel Digital Processor System for Particle Image Velocimetry. Meas. Sci. Tehcnol, 4, 1993, 619–626.

7. Prassad, A.K., Adrian, R.J., Landreth, C.C., and Offutt, P.W.: Effect of Resolution on the Speed and Accuracy of Particle Image Velocimetry Interrogation. Exp, Fluids, 13, 1992, 105–116.

8. Tennekes, H., and Lumley, J.L.: A First Course in Turbulence. MIT Press, Cambridge, MA, 1972.

9. Landreth, C.C., and Adrian, R.J.: Impingement of a Low Reynolds Number Turbulent Circular Jet onto a Flat Plate at Normal Incidence. Experiments in Fluids, 9, 74–84 (1990).

10. Reuss, D.L., Adrian, R.J., Landreth, C.C., French, D.T., and Fansler, T.D.: Instantaneous Planar Measurements of Velocity and Large-Scale Vorticity and Strain Rate in an Engine Using Particle-Image Velocimetry. SAE 890616, International Congress and Exposition, Detroit, MI, Feb27–March 3, 1989.

11. Batchelor, G.K.: The Theory of Homogeneous Turbulence. Cambridge University Press, 1953.